Structure-guided PEGylated fibroblast growth factor 2 variants accelerate wound healing with improved stability

Jian Sun[1], Jiamin Wu[1], Hui Jin[2], Te Ying[1], Wei Jin[1], Miaojuan Fan[1], Jianhui Zhou[3], Hui Chen[3], Litai Jin[1], and Jie Zhou[1]

[1]Wenzhou Medical University
[2]Wenzhou Medical University First Affiliated Hospital
[3]Taizhou Hospital of Zhejiang Province

May 5, 2020

Abstract

Background and Purpose Fibroblast growth factor 2 (FGF2) plays an important role in multiple physiological functions such as tissue repair. However, it has a short half-life in vivo, thus limiting its clinical application. Experimental Approach Based on the crystal structure of FGF2, surface-exposed sites near the receptor and heparin binding region or separated from both binding regions, were selected and PEGylated to investigate the effects of these sites on protein stability and bioactivity. The efficacy of FGF2 conjugates for wound healing in vitro was screened by cell proliferation, migration of human dermal fibroblasts (HDFs) and human umbilical vein endothelial cells (HUVECs). Angiogenesis activity was assessed by tube forming and aortic ring assays. The stability was confirmed in plasma and wound fluid. The in vivo wound healing of FGF2 conjugates were further evaluated on a cutaneous wound model using H&E, IHC, IF, and collagen staining. Key Results Compared with native FGF2, all PEG-FGF2 conjugates exhibited significantly improved stability in plasma and wound fluid. Compound 6 more effectively promoted proliferation and migration in HDFs and HUVECs than FGF2, and exhibited excellent angiogenesis and wound healing activity in vivo. However, conjugates with the PEGylated sites near the receptor and heparin binding regions showed some reduction in bioactivity, with a greater loss of bioactivity for protein with site near the heparin binding domain. Conclusion and Implications Heparin binding domain may be a key contribution region to activity of FGF2. Compound 6 is a potential therapeutic candidate for wound healing, deserving further investigation.

Abbreviations

FGF2: Fibroblast growth factor 2

PEG: Poly (ethylene) glycol

ERK1/2: Extracellular signal–regulated kinases 1 and 2

p-ERK1/2: phosphorylated ERK1/2

mPEG-MAL: monomethoxy PEG-maleimide

HDFs: Human dermal fibroblast cells

HUVECs: Human umbilical vein endothelial cells

CCK-8: cell counting kit-8

MMPs: metalloproteinases

HG: high glucose

H&E: Hematoxylin and Eosin

PCNA: Proliferating cell nuclear antigen

1. Introduction

Fibroblast growth factor 2 (FGF2) is a member of the heparin-binding growth factor (HBGF) family, and is widely expressed in development and adult tissues (Nguyen *et al.* , 2013). FGF2 is a potent stimulator of cell proliferation, differentiation, and migration of multiple cell types, playing an essential role in embryonic development (Slack*et al.* , 1987), tissue repair (Maddaluno *et al.* , 2017), and angiogenesis (Chu *et al.* , 2011; Corseaux *et al.* , 2000). FGF2 can be used to accelerate the healing of both acute and chronic wounds. However, it has a short circulation half-life due to rapidly protease degradation, kidney filtration, and antigenic response, limiting its clinical application. Thus, increasing the stability of FGF2 is required to improve its application potential.

Although there are many chemical modification approaches to address stability, poly (ethylene) glycol (PEG) modification has been well demonstrated as an effective strategy to improve stability and biocompatibility of proteins (Brocchini *et al.* , 2008; DeFrees*et al.* , 2006; Krall *et al.* , 2016). PEG is a substance that has been designated by the Food and Drug Administration (FDA) as "Generally Recognized as Safe (GRAS)" (Parnaud *et al.* , 1999), and a variety of PEGylated proteins have been approved for use by FDA (Dozier *et al.* , 2015). The most widely used PEG modification method is to engineer a single cysteine into a protein, and then rapidly and quantitatively react this cysteine with a PEG-maleimide group, thus forming a protein-PEG conjugate (Foley *et al.* , 2007; Rosen*et al.* , 2017). Cysteine is an ideal target for site-specific protein modification due to its typical low abundance in proteins and the high nucleophilicity of the sulfhydryl side chain (Bernardim*et al.* , 2016). Previous efforts using site-selective PEGylation of cysteine residues have resulted in modified proteins with improved pharmacokinetics and retained biological activity (Dozier *et al.* , 2015).

The crystal structure of the FGF2-FGFR-Heparin ternary complex shows that FGF2 activity depends on the heparin-dependent formation of 2:2 FGF2-FGFR dimer complex (Beenken *et al.* , 2012). Heparin facilitates FGF-FGFR dimerization by binding both FGF and FGFR, and thereby promoting and stabilizing the protein-protein contacts between ligand and receptor (Beenken *et al.* , 2009). Obviously, the receptor binding region and heparin-binding region are important regions for the activity of FGF2. However, there has been little detailed study of structure-activity relationships in FGF2. Previous efforts to modify FGF2 focused on the protein's N-terminus or chemical modification of two surface-exposed cysteines (Decker *et al.* , 2016; Kang *et al.* , 2010), but the resulting long-acting FGF2 conjugates exhibited reduced bioactivity. Therefore, a rational modification strategy based on the structure to select optimal sites on the protein for cysteine mutation may be more effective to obtain PEGylated proteins that retain biological activity.

To identify suitable modification sites, four surface-exposed sites, including two sites near the heparin- and FGFR-binding regions and two native cysteines were selected and substituted by cysteine or alanine, and PEG-FGF2 conjugates were synthesized and purified. Structure-activity analysis and long-acting characteristics of these conjugates were explored using *in vitro* and *in vivo* wound healing models.

2. Materials and Methods

2.1 Expression and purification of FGF2 and its variants

Recombinant human fibroblast growth factor 2 (FGF2) and its variants were expressed in the *E. coli* system as previously reported (Huang *et al.* , 2017). The Fast Mutagenesis System Kit (TransGen Biotech, Beijing, China) was used to introduce mutations into native FGF2 expression vector in order to generate the variant constructs. BL21 (DE3) competent cells were transformed with the expression vectors and cultured in LB medium with shaking at 37 °C to an absorbance of 0.5 at 600 nm, then protein expression was induced by addition of 1 mM isopropyl 1-thio-D-galactopyranoside (IPTG) and continued incubation for 4 h. Cell

pellets were lysed in 150 mM NaCl, 10% glycerol, 25 mM Hepes-NaOH, pH 7.5, and 5 mM EDTA. The cell suspensions were centrifuged at 12,000 rpm for 30 min at 4 °C, and the soluble lysate fractions containing FGF2 variants proteins were purified by heparin affinity column (Hitrap Heparin HP column, 5 ml), followed by further separation by Superdex 75 10/300 gel filtration column. The purity of FGF2 variants was confirmed by 12% sodium dodecyl sulfate polyacrylamide gel electrophoresis (SDS-PAGE). The purified FGF2 variants were concentrated using Amicon Ultra Centrifugal Filters and the resulting concentrations were determined by absorbance measurements using a Nanodrop spectrophotometer. The detailed amino acid sequences of these proteins were shown in **supplemental table 1** .

2.2 Site-specific PEGylation of FGF2 conjugates and purification

The PEGylated FGF2 conjugates were generated by site specific PEGylation using mPEG-Maleimide (mPEG-MAL, 5kDa). We optimized the reaction conditions, including temperature, reaction time, and the PEG-to-FGF2 molar ratio as 4 °C a PEG-to-FGF2 molar ratio of 4, and 1 h, respectively. The yield of PEGylation was confirmed by SDS-PAGE.

To separate the PEGylated FGF2 conjugates from unreacted FGF2 and mPEG-MAL, reaction mixtures were applied at a rate of 5 mL/min to a Heparin HP column (5 mL bed volume) pre-equilibrated with 15 column volumes (CVs) of binding buffer (25 mM HEPES buffer, pH 7.5). The column was then washed with 10 CVs of binding buffer, and then the protein was eluted with buffer A (25 mM HEPES buffer, pH 7.5 and buffer B (25 mM HEPES buffer, pH 7.5, 2 M NaCl) over 30 CVs. Eluted fractions were collected and analyzed by SDS-PAGE.

2.3 Cell culture

Human umbilical vein endothelial cells (HUVECs) were purchased from Lonza and cultured in endothelial cell growth medium-2 (EGM-2, Lonza, Cat#CC-3156 & CC-4176) at 37 °C in 5% CO_2 before the experiment. Subconfluent cells obtained after 5-7 passages were used in the following experiments. Twelve h prior to cell culture, culture media was removed and replaced with phenol red-free low-glucose DMEM (Gibco, Cat#11054020) supplemented with 1% calf serum (Gibco, Cat#16010159). HUVECs were then transferred to EGM-2 with high glucose (HG, 33 mM) in the presence of FGF2 or PEG-FGF2 conjugates (10 ng·mL^{-1}) for 72 h. PBS (Gibco, Cat#10010) was used as a negative control (untreated cells). The media was replaced every 24 h. All experiments were independently carried out at least three separate times.

Human dermal fibroblasts (HDFs) were separated from human foreskin samples obtained from volunteers, as previously described (Takahashi *et al.* , 2006). HDFs were cultured in DMEM supplemented with 5.5 mM glucose, 10% FBS, and 1% penicillin-streptomycin, and were passaged by using 0.25% trypsin (Gibco) when cell confluence reached ˜80%. Primary human fibroblasts at passage 5-6 were used in the experiments described below.

2.4 Cell proliferation assay

Cell proliferation was detected using a Cell Counting Kit-8 (CCK-8; Biosharp; Cat#BS350A). HUVECs and HDF cells were separately seeded 2×10^3/well in 96-well plates. The cells were allowed to adhere for 12 h at 37 °C in 5% CO_2. After 12 h, the medium was removed and replaced with 100 μL of FGF2 or PEG-FGF2 conjugates for 24 h before addition of CCK-8 solution (10 μL) to each sample. The absorbance was measured at 450 nm using a microplate reader (Molecular Devices, USA). Cell proliferation assays were performed in triplicate.

2.5 *In vitro* wounding assay

A previously described wound healing scratch assay was used to assess cell migration (Das *et al.* , 2018). Cells were plated at a density of 160000 cells/ml in 24-well culture plates and incubated at 37 °C in 5% CO_2 until formation of a confluent monolayer. Cells were then scratched once per well, vertically, with a 200 μL plastic pipette tip to create an artificial wound. After washing twice to remove cellular debris by PBS, cells were treated with 10 ng·mL^{-1} FGF2, PEG-FGF2 conjugates, or PBS control. The same fields were

photographed every 12 h by Nikon Eclipse Ni light microscopy and the areas of cell migration were calculated with ImageJ Software (National Institutes of Health, Bethesda, MD, USA). The percent migration at each time point was defined as the ratio of (the original area - the open area at 24 h) to the original area. All the experiments were performed in triplicate.

2.6 Protein stability in rat plasma

The stability of the prepared compounds was assessed in rat plasma collected from adult male Sprague Dawley (SD) rats, as previously described (Zhou *et al.* , 2017). Briefly, plasma was stored at -80 °C until needed. *In vitro*stability of FGF2 and PEG-FGF2 conjugates was measured using initial concentrations of 1000 ng·mL^{-1} of each protein in mouse plasma at 37 °C. Aliquots of 100 μL of plasma were removed at 0, 2, 4, 6, and 8 h time points and subjected to solid phase extraction on a Waters Oasis HLB 96-well plate (Milford, MA). The dynamic levels of FGF2 or PEG-FGF2 conjugates in the plasma were measured by human FGF2 immunoassay ELISA kit (Abcam, Cambright, UK) using a standard curve.

2.7 Protein stability in wound fluid

Wound fluid was collected as previously described (Grinnell *et al.* , 1992). The stabilities of FGF2 and PEG-FGF2 conjugates were investigated in wound fluids as previously described (Olekson *et al.* , 2015). Briefly, FGF2 and PEG-FGF2 conjugates were added to wound fluids collected within 1 day after scalding and further incubated for 48 h at 37 °C. After centrifugation at 12000 rpm, supernatants were collected for bioactivity test. The residual amounts of FGF2 retained for FGF2 and the three PEG-FGF2 conjugates were quantitatively analyzed by ELISA.

2.8 Angiogenesis (tube formation) assay *in vitro*

The *in vitro* angiogenic activity of HUVECs was determined by Matrigel tube formation assay. After the experimental period described above, HUVECs were stained with a cell-permeable dye, calcein (Cat#354216, Corning incorporated, USA), for 30 min and transferred to 24-well plates precoated with 150 μL/well growth factor-reduced Matrigel (Cat#354234, Corning incorporated, USA) and then incubated at 37°C in a cell culture incubator. After 12 h incubation, capillary-like tube formation was observed with a computer-assisted microscope (EVOS, Thermo Fisher Scientific, USA). Tube formation was defined as a tube-like structure exhibiting a length four times its width. The tube lengths in duplicate wells were counted and averaged using ImageJ software.

2.9 Aortic ring assays

To establish the direct action of FGF2 and PEG-FGF2 conjugates on vascular tissue, the thoracic aortae of 8-week-old mice from each group were isolated surgically, cleaned, and dissected into 0.5 mm rings. Rings were then embedded in 1 mg/mL of type I collagen (Millipore, Cat#08-115) in a 96-well plate as described previously (Baker *et al.* , 2011). The embedded rings were cultured in HG (33 mM) serum-free endothelial basal medium (EBM) (Lonza, Cat#CC-3121) in the presence of FGF2 or PEG-FGF2 conjugates. During the exponential growth phase, angiogenic response data were obtained by counting the endothelial microvessel sprouts growing out from the cultured rings. Before the regression phase, rings were fixed with 4% (w/v) paraformaldehyde for 30 min. Pictures were taken on day 12 with a computer assisted microscope (Eclipse Ni, NIKON), and the total number of branches was counted using ImageJ (National Institutes of Health, USA).

2.10 Animals

Male C57BL/6 mice were purchased from the Model Animal Research Center of Nanjing University (Nanjing, China) and were allowed to acclimate to the facilities for at least 7 days. All mice were housed under standard laboratory conditions of temperature at 21 +- 2 degC, relative humidity 50 +- 15%, and 12 h light/darkness cycles, with water and food freely available. Animal studies are reported in compliance with the ARRIVE guidelines (Kilkenny *et al.* , 2010) and the editorial on reporting animal studies (McGrath *et al.* , 2015) with the recommendations made by the *British Journal of Pharmacology* . All experimental procedures and

methods in this research were approved by the Institutional Animal Care and Use Committee of Wenzhou Medical University.

2.11 *In vivo* wound closure assay

C57BL/6 male mice were anesthetized by intraperitoneal injection of 4% chloral hydrate. The skin hair on the backs of mice was removed using a shaving machine and depilatory creams. Alcohol was used to rinse the skin, and silicone rings with an internal diameter of 8 mm and thickness of 0.5 mm were stitched on the skin. Two full-thickness wounds per mice were made on the dorsal skin with surgical scissors. After surgery, the wounds were treated with 10 μL FGF2 or PEG-FGF2 conjugates (10 μg·ml^{-1}, produced by Wenzhou Medical University gene engineering laboratory) or PBS once a day. Digital photographs of the wound area were taken on days 0, 3, 5, and 7 and the wound areas were measured using ImageJ software. The ratio of wound healing was defined as the ratio of (the original wound area - the wound area on the collected day) to the original wound area. Skin wound samples were collected 7 days after injury and fixed in 4% paraformaldehyde for histological and immunofluorescence analyses.

2.12 Immunoblot analysis

Protein concentrations were determined using a BCA Kit (Protein Assay Kit, Beyotime Biotechnology, Shanghai, China). 30 μg of total protein was loaded and separated by SDS-PAGE and transferred to PVDF membranes (Millipore, Germany). Membranes were blocked with 5% (w/v) milk (Bio-Rad) in Tris-buffered saline containing 0.1% (v/v) Tween 20 (TBST) at room temperature for 1 h. Each nitrocellulose membrane was incubated with primary antibodies to phospho-p44/42 MAPK (Erk1/2) (Cell Signaling Technology; Cat#4370; 1:1000 dilutions), p44/42 MAPK (Erk1/2) (Cell Signaling Technology; Cat#9102; 1:1000 dilutions), GAPDH (Cell Signaling Technology; Cat#2118; 1:1000 dilutions) at 4 °C overnight. After three washes with TBST, Immune-reactive bands were detected by incubating with horseradish peroxidase (HRP) conjugated secondary antibodies (Santa Cruz Biotechnology; Cat#sc-2004; 1:3000 dilutions) at room temperature for 1 h. Then protein bands were incubated using the EasySee western Blot Kit (TransGen Biotech, Beijing, China) and visualized using enhanced chemiluminescence (ECL) reagents (Bio-Rad, Hercules, CA). Densitometric analysis was performed using Image J software (NIH, USA). The immune-related procedures used comply with the recommendations made by the *British Journal of Pharmacology* (Alexander *et al.* , 2018).

2.13 Histological analysis

Skin tissues were fixed with 4% paraformaldehyde solution for 24 h, and then embedded in paraffin. Skin tissue was sliced into sections 5 μm in thickness, followed by H&E or Masson's trichrome staining according to the standard protocols. Tissue images were captured using Nikon Eclipse Ni light microscopy.

2.14 Immunohistochemistry staining

Paraffin skin sections (5 μm in thickness) were deparaffinized and rehydrated, and subsequently treated with antigen retrieval solution for 6 min at 96 °C. The sections were stained with PCNA antibody (Abcam; Cat#ab29; 1:200) at 4 °C overnight, and then reprobed with goat-anti-rabbit HRP-conjugated antibody for 2 h at room temperature. All antibodies were diluted with PBS containing 1% BSA. The staining was visualized by reacting with 3, 3-diaminobenzidine (1:20) (DAB; Sigma Chemical Co., USA), and then the nuclei were stained with hematoxylin (Solarbio Science & Technology, China). Results were evaluated by Nikon Eclipse Ni light microscopy.

2.15 Immunofluorescence staining

For staining of HUVECs, cells cultured in 6-well plates were fixed with 4% paraformaldehyde for 30 min and permeabilized with 0.5% Triton-X 100 (Solarbio Science & Technology, China) for 15 min. Next, samples were incubated with 5% BSA for 30 min at room temperature to block nonspecific binding and then incubated with Ki67 (Cell Signaling Technology; Cat#11882; 1:200) at 4 °C overnight. Alexa Fluor 488-conjugated anti-mouse IgG secondary antibody (Abcam; Cat#ab150113; 1:200) was then added and incubated for 1 h

at room temperature. The nuclei were labeled with DAPI for 10 min, and then images were captured by Leica SP8 confocal microscopy (Leica, Wetzlar, Germany).

For quantification of the CD31 positive areas, sections were stained with anti-CD31 antibody (Abcam; Cat#ab24590; 1:100) and then incubated with Alexa Fluor 647-conjugated anti-rabbit IgG secondary antibody (Abcam; Cat#ab150115, 1:200) for 60 min at room temperature. Subsequently, cell nuclei were stained with DAPI. All fluorescent images were taken using a Leica SP8 confocal microscopy (Leica, Wetzlar, Germany).

Statistical Analysis

Statistical analysis was performed using Graphpad Prism 8.0 software (GraphPad, San Diego, CA). Data are presented as mean values ± SD. Each set of experiments was repeated independently at least three times with comparable results. Student's t -tests were performed to determine the significance of differences between pairs. One-way analysis of variance (ANOVA) was utilized to determine significant differences between multiple groups. P <0.05 was considered statistically significant.

3. Results

3.1 Rational design of FGF2 variants

Selection of an appropriate modification site is important for the retention of biological activity of PEGylated proteins. The surface of FGF2 contains two native cysteines, Cys69 and Cys87, which are surface exposed and spatially distal from both the receptor and heparin binding regions. We separately mutated each cysteine to alanine, thus generating two FGF2 containing only a single surface-exposed cysteine (compounds**1** and **2**). And two surface-exposed residues, Lys129 and Phe17, near the heparin- and receptor-binding regions, respectively, were also changed to cysteines (compounds **3** and **4**) (**Figure 1A**). The resulting FGF2 variants, each containing a single cysteine for PEGylation, were engineered and tested: $FGF2^{C69A}$ (compound **1**), $FGF2^{C87A}$ (compound **2**), $FGF2^{C69A/C87A/F17C}$ (compound **3**), and $FGF2^{C69A/C87A/K129C}$ (compound **4**) (**Figure 1 B and E**).

The activation of extracellular signal-regulated kinases 1 and 2 (ERK1/2) is a key point of convergence for many signaling pathways, and the biological response of extracellular stimuli including FGF2 requires ERK1/2 activation (Johnson *et al.* , 2002). Hence, signaling of the ERK1/2 pathway was evaluated by immunoblotting to assay the activity of FGF2 and its mutants. The cellular phosphorylated ERK1/2 (p-ERK1/2) levels were increased with native FGF2 compared with the control group, and the same increase occurred with compounds **1** and **2**(**Figure 1 C-D**). A slight reduction in the cellular level of p-ERK1/2 was observed for compounds**3** and **4** (**Figure 1 E-F**). These results indicated that both the receptor- and heparin-binding regions are indeed important for FGF2 activity and that single site mutation distal from the binding domains has little effect on protein activity.

3.2 Site-specific PEGylation of FGF2 variants

We used 5kDa monomethoxy PEG-maleimide (mPEG-MAL) to specifically modify the surface-exposed cysteine on FGF2 and the mutants, as shown in**Figure 2A** . Three mono-PEGylated FGF2 conjugates were generated and named as PEG-$FGF2^{C69A/C87A/F17C}$ (compound**5**), PEG-$FGF2^{C87A}$ (compound **6**), and PEG-$FGF2^{C69A/C87A/K129C}$ (compound **7**) (**Figure 2B)** . SDS-PAGE analysis confirmed the purification of these PEGylated FGF2 conjugates. A single band corresponding to protein with an apparent Mw of 25kDa appeared after PEGylation (**Figure 2C**). After purification, the ERK1/2 pathway activity was measured. All PEG-FGF2 conjugates and native FGF2 exhibited higher ERK1/2 phosphorylation activity than that of the PBS control. In addition, compared with FGF2, compound **5** and **6** induced about 1.5- and 2- fold higher phosphorylation, and compound **7**exhibited a significant reduction in phosphorylation (**Figure 2 D-E**). The decreased activity of compound **7** , in which PEGylation would occur at the engineered cysteine near the heparin-binding region, suggests that steric hindrance of the PEG polymers can interfere with binding between heparin and the receptor. The observed sensitivity of the heparin-binding region suggests designs

that do not interfere with this region of the protein may result in FGF2 conjugates with increased activity retention and stability after site-specific PEGylation.

3.3 Screening of conjugates in cell proliferation activity and scratch wound healing assays

The efficacy of FGF2 conjugates for wound healing can be assessed by measuring the cell proliferation, migration, and vasculogenesis of dermal fibroblasts and endothelial cells (Rabuka, 2010; van Horssen*et al.* , 2006). Here, human dermal fibroblast cells (HDFs) and human umbilical vein endothelial cells (HUVECs) were used as *in vitro* models to screen and compare the bioactivities of these conjugates.

First, the dose-dependent effects of PEG-FGF2 conjugates on cell proliferation of HUVECs were investigated by CCK-8 assay. The cells were incubated with various treatment conditions at concentrations of 0.1, 1, and 10 ng*mL^{-1} of protein for 24 h. Compound **6** promoted significantly greater cell proliferation than all the other compounds, including native FGF2, even at a low concentration (0.1 ng*mL^{-1}), with the highest pro-proliferation activity at a concentration of 10 ng*mL^{-1} (**Figure 3A**). We also evaluated the cell proliferation activity of these conjugates by immunofluorescence staining for Ki67-positive HUVECs at 10 ng*mL^{-1}. Compounds **5** and **6** showed a significant increase in the number of Ki67-positive cells compared with the PBS control, with a bigger effect for compound **6** than that for FGF2 (**Figure 3 B-C**).

Next, a scratch wound healing assay was performed to evaluate the effects of PEG-FGF2 conjugates on cell migration of HUVECs. A scratch was made through a confluent layer of growth factor starved cells followed by the application of different compounds. Compared with FGF2 treatment, a significant reduction in wound area was observed upon treatment with compound **6** at 24 h, with migration of HUVECs increased by ˜163% compared to only ˜108% for FGF2 (**Figure 3 D-E**). The activity of compound **5** is similar to that of FGF2. Overall, these results indicate that compound **6** can notably promote proliferation and migration of HUVECs relative to unmodified FGF2.

The same compounds were also tested using human dermal fibroblasts (HDFs). There was increased proliferation and migration of HDFs after treatment with compound **6** relative to treatment with other protein conjugates (**Figure 4 A-C**). These results were consistent with the results for HUVECs, which indicated improved bioactivity of compound **6** to promote cell proliferation and scratch wound healing in both dermal fibroblasts and endothelial cells, which may be attributed to the long-acting effect of PEGylation.

3.4 Stability studies of PEG-FGF2 conjugates

To verify whether site-specific PEGylation improves the stability of FGF2 conjugates, SD rat plasma and mice wound fluid were used.

Compounds **5** , **6,** and **7** were first incubated with rat plasma over 24 h and compared with FGF2 incubation. Solid-phase extraction was conducted at different time points, and the remaining FGF2 was analyzed using ELISA Kit to examine plasma stability (**Figure 5A**). The results showed rapid degradation of native FGF2 in plasma, with its concentration decreased to less than 10% of the initial value within 30 min and complete degradation within 1 h at 37 degC. In contrast, all PEG-FGF2 conjugates showed enhanced stabilities relative to the unmodified FGF2. After 2 h of incubation in plasma, the residual FGF2 percentages of compounds **5** , **6,** and**7** were about 66%, 93% and 90% of the initial concentrations, respectively. After 8 h of incubation, about 33%, 76%, and 58% of the initial concentrations remained for compounds **5** , **6,**and **7** , respectively. The data indicate that site-specific PEGylation can significantly improve the stability of FGF2 in plasma.

Acute wound fluid is generally rich in metalloproteinases (MMPs), especially MMP2 and MMP9 subtypes, within the initial 3 days after scald (Xu *et al.* , 2018), which may result in elevated levels of proteases that can rapidly degrade exogenous growth factors (Ladwig*et al.* , 2002). Therefore, the stability of PEG-FGF2 conjugates was further quantitatively analyzed by ELISA Kit after incubation in wound fluids collected within 1 day after scald (**Figure 5B**). As expected, FGF2 mixed with wound fluid was degraded rapidly, for a remaining FGF2 rate of 4.47 +- 0.95% after incubation in wound fluid for 24 h. Compounds **5** , **6,** and **7** were more stable, with remaining FGF2 rates of 32.00 +- 7.94%, 63.33 +- 3.51%, and 49.33 +- 5.13%

respectively. These results indicate that all PEG-FGF2 conjugates exhibit obviously increased stability in wound fluids compared to unmodified FGF2.

Taken together, these results demonstrate that site-specific PEGylation can effectively protect FGF2 from degradation for increased stability. Among the tested PEG-FGF2 conjugates, compound **6** exhibited the strongest stability.

3.5 Effect in endothelial impairment protection and angiogenesis both *in vitro* and *ex vivo*

To assay the protective effect of PEG-FGF2 conjugates against endothelial impairment *in vitro* , we explored tube-forming activity in HUVECs exposed to high glucose (HG, 33 mM) medium treated with compounds **5** , **6** , and**7** , or controls (PBS and FGF2) for 72 h. We found significantly impaired tube-forming activity in HUVECs exposed to HG, with significant enhancement by compound **6** compared to native FGF2 (**Figure 6 A and C**). This result showed that improved tube-forming activity by compound **6** in HUVECs exposed to HG.

To further characterize the endothelial angiogenesis function of PEG-FGF2 conjugates, an *ex vivo* model was next performed (Brill*et al.* , 2004). The aortic rings from C57BL/6 mice were cultured in medium containing HG (33 mM) with either FGF2 or PEG-FGF2 conjugates. Aortic rings cultured in HG medium exhibited dramatically impaired sprouting function, but the sprouting function was well preserved by FGF2 and compound **6** (**Figure 6 B and D**). The tube lengths of samples incubated with compound **6** were longer than those of samples incubated with native FGF2. Compounds **5** and**7** promoted angiogenesis to some degree. These results confirm that compound **6** exhibits the strongest vascular regeneration activity in HG medium, implicating its potential application in diabetic wound healing.

3.6 Assessment of PEG-FGF2 conjugates on skin wound healing*in vivo*

To confirm the positive wound healing effects of PEG-FGF2 conjugates*in vivo* , wound closure was measured at days 0, 3, 5, and 7. These PEF-FGF2 conjugates showed a certain function of wound healing compared with the PBS control. Consistent with our *in vitro* results, topical administration of 100 ng compound **6** significantly accelerated wound healing compared to PBS treatment over the course of the healing process (**Figure 7A**). Quantitatively evaluation of wound healing rate revealed that compound **6** was more effective in wound healing compared to FGF2 (**Figure 7B**).

The pathological morphology and diameters of cutaneous wounds at day 7 after surgery were assessed with Hematoxylin and Eosin (H&E) staining. Wounds treated with compound **6** showed increased healing and shorter diameter. This result further confirms the effectiveness of compound **6** in cutaneous wound healing (**Figure 7C**). Collagen deposition after treatments was also detected by Masson's trichrome staining. As shown in **Figure 7 D-E** , different degrees of collagen deposition were observed for these compounds. Sections of wounds treated by compound **6** exhibited significantly higher collagen deposition compared with wounds treated with unmodified FGF2, indicating the improved therapeutic effect of compound **6** . However, wound sections of compounds **5** and **7** exhibited very little collagen deposition, consistent with the results of H&E staining. The results together demonstrate that compound **6** is more effective in promoting cutaneous wound healing *in vivo* .

3.7 Promotion of angiogenesis and proliferation *in vivo*

Angiogenesis is a complicated physiological process, playing an important role in wound healing (Potente *et al.* , 2011). *In vivo* , the observation of new vessels is a direct way to evaluate angiogenic activity. CD31 is a key biomarker of endothelial cells in blood vessels, and neovascularization was evaluated via immunofluorescence staining of CD31 in the cutaneous wounds. Newly formed vessels were detected in all groups, with higher abundance for FGF2 and compound **6** treatments (**Figure 8A**). There was significantly better vessel density in the wound beds treated with compound **6** (57.67 +- 7.50 / mm^2) than that in wounds treated with FGF2 (31.33 +- 4.16 / mm^2) (**Figure 8B**), suggesting compound **6** was more effective in promoting angiogenesis in the wound bed.

The pro-proliferation activity *in vivo* around the wound edge was further verified by immunohistochemistry staining of Proliferating cell nuclear antigen (PCNA). Consistent with the *in vitro* cellular proliferation result, there were few PCNA positive cells around the wound in PBS (control) mice. In contrast, an increased number of proliferating cells were detected in the epidermis and hair follicle for mice treated with compounds **5** , **6,** and **7,** or FGF2, with 1.5-fold more proliferating cells for compound **6**treatment compared to treatment with FGF2 (**Figure 8 C-D**).

All these data demonstrate that these FGF2 conjugates can effectively promote the proliferation and migration of epithelium and dermal cells, and enhance the activity of vascular regeneration, hence accelerating cutaneous wound healing (**Figure 8E**). Compound **6**exhibits the most potent wound healing with good stability.

4. Discussion

As a potent mitogenic factor, FGF2 has been extensively explored for potential application in wound healing (Li *et al.* , 2016). However, FGF2 can be rapidly degraded by enzymes and rapid renal filtration *in vivo,* thereby limiting its clinical value. Site-specific protein PEGylation can minimize reduction in biologic activity while improving pharmacokinetic properties.

In this study, we found that the mutation of either cysteine on the surface of FGF2 is not detrimental to protein activity, which is consistent with the results of previous study (Kang *et al.* , 2010). However, the mutation of surface sites near the heparin and receptor binding domains slightly reduced protein activity. The results indicate that surface-exposed sites that are spatially separated from both binding domains may be better candidates for modification. The three conjugates obtained by PEGylation showed different bioactivities. In particular, compound **6** , PEGylated at a site spatially separated from both the heparin and receptor binding regions, exhibited the strongest activity. Compound **5** with the PEGylated site close to the receptor binding domain showed the second-highest activity, and compound **7** with the site of PEGylation near the heparin binding domain was the weakest. The heparin binding region may be more conserved, and steric hindrance due to the presence of PEG polymers may affect heparin binding. Heparin makes numerous contacts with both FGF2 and FGFR, thus augmenting FGF2-FGFR binding (Sarabipour *et al.* , 2016), and it also interacts with FGFR in the 1:1 FGF2-FGFR complex to facilitate FGF2-FGFR dimerization, with increased intracellular receptor tyrosine kinase activity that triggers various downstream signaling pathways (Schlessinger *et al.* , 2000). In addition to these roles in both FGFR binding and dimerization, heparin may function directly as a receptor for FGF2 (Chua *et al.* , 2004).

In summary, based on the structure of FGF2, four surface-exposed sites close to or far from the receptor/heparin binding regions, were selected and mutated to cysteine or alanine, allowing assay of PEGylation of specific residues. All PEGylated FGF2 conjugates exhibited significantly improved stability. Among these conjugates, compound **6** , modified far from the heparin and receptor binding domains, exhibited the strongest biological activity. This conjugate effectively promoted the proliferation and migration of epithelium and dermal cells, and enhanced the activity of vascular regeneration to accelerate wound healing. These results together suggest that compound **6** may be a promising candidate for the treatment of cutaneous wounds. Overall, structure-guided site-specific PEGylation offers a good strategy to develop improved proteins for use as therapeutics.

Disclosure

All the authors declared no competing interests.

Author contributions

JS, JW, HJ, TY, WJ, MF, JZ, HC, LJ and JZ researched the data. JW, LJ and JZ contributed to the initial discussion and design of the project. JS and JZ wrote the manuscript.

Acknowledgments

This research was supported by National Natural Science Foundation of China (Grant No. 81800725), Science and Technology Plan Project of Taizhou (Grant No. 1801ky54, 1902ky50), Science and Technology Project of Wenzhou (Grant No. Y20160162).

References

Alexander SPH, Roberts RE, Broughton BRS, Sobey CG, George CH, Stanford SC*, et al.* (2018). Goals and practicalities of immunoblotting and immunohistochemistry: A guide for submission to the British Journal of Pharmacology. Br J Pharmacol 175**:** 407-411.

Baker M, Robinson SD, Lechertier T, Barber PR, Tavora B, D'Amico G*, et al.* (2011). Use of the mouse aortic ring assay to study angiogenesis. Nat Protoc 7**:** 89-104.

Beenken A, Eliseenkova AV, Ibrahimi OA, Olsen SK, & Mohammadi M (2012). Plasticity in interactions of fibroblast growth factor 1 (FGF1) N terminus with FGF receptors underlies promiscuity of FGF1. J Biol Chem 287**:** 3067-3078.

Beenken A, & Mohammadi M (2009). The FGF family: biology, pathophysiology and therapy. Nat Rev Drug Discov 8**:** 235-253.

Bernardim B, Cal PM, Matos MJ, Oliveira BL, Martinez-Saez N, Albuquerque IS*, et al.* (2016). Stoichiometric and irreversible cysteine-selective protein modification using carbonylacrylic reagents. Nat Commun 7**:** 13128.

Brill A, Elinav H, & Varon D (2004). Differential role of platelet granular mediators in angiogenesis. Cardiovasc Res 63**:** 226-235.

Brocchini S, Godwin A, Balan S, Choi JW, Zloh M, & Shaunak S (2008). Disulfide bridge based PEGylation of proteins. Adv Drug Deliv Rev 60**:** 3-12.

Chu H, Gao J, Chen C, Huard J, & Wang Y (2011). Injectable fibroblast growth factor-2 coacervate for persistent angiogenesis. Proc Natl Acad Sci 108**:** 13444-13449.

Chua CC, Rahimi N, Forsten-Williams K, & Nugent MA (2004). Heparan Sulfate Proteoglycans Function as Receptors for Fibroblast Growth Factor-2 Activation of Extracellular Signal–Regulated Kinases 1 and 2. Circ Res 94**:** 316-323.

Corseaux D, Meurice T, Six I, Rugeri L, Ezekowitz MD, Rouvier P*, et al.* (2000). Basic fibroblast growth factor increases tissue factor expression in circulating monocytes and in vascular wall. Circulation 101**:** 2000-2006.

Das A, Huang GX, Bonkowski MS, Longchamp A, Li C, Schultz MB*, et al.* (2018). Impairment of an Endothelial NAD(+)-H2S Signaling Network Is a Reversible Cause of Vascular Aging. Cell 173**:** 74-89 e20.

Decker CG, Wang Y, Paluck SJ, Shen L, Loo JA, Levine AJ*, et al.*(2016). Fibroblast growth factor 2 dimer with superagonist in vitro activity improves granulation tissue formation during wound healing. Biomaterials 81**:** 157-168.

DeFrees S, Wang ZG, Xing R, Scott AE, Wang J, Zopf D*, et al.*(2006). GlycoPEGylation of recombinant therapeutic proteins produced in Escherichia coli. Glycobiology 16**:** 833-843.

Dozier JK, & Distefano MD (2015). Site-Specific PEGylation of Therapeutic Proteins. Int J Mol Sci 16**:** 25831-25864.

Foley TL, & Burkart MD (2007). Site-specific protein modification: advances and applications. Curr Opin Chem Biol 11**:** 12-19.

Grinnell F, Ho CH, & Wysocki A (1992). Degradation of fibronectin and vitronectin in chronic wound fluid: analysis by cell blotting, immunoblotting, and cell adhesion assays. J Invest Dermatol 98**:**410-416.

Huang Z, Tan Y, Gu J, Liu Y, Song L, Niu J*, et al.* (2017). Uncoupling the Mitogenic and Metabolic Functions of FGF1 by Tuning FGF1-FGF Receptor Dimer Stability. Cell Rep 20**:** 1717-1728.

Johnson GL, & Lapadat R (2002). Mitogen-activated protein kinase pathways mediated by ERK, JNK, and p38 protein kinases. Science 298**:** 1911-1912.

Kang CE, Tator CH, & Shoichet MS (2010). Poly(ethylene glycol) modification enhances penetration of fibroblast growth factor 2 to injured spinal cord tissue from an intrathecal delivery system. J Control Release 144**:** 25-31.

Kilkenny C, Browne W, Cuthill IC, Emerson M, Altman DG, & Group NCRRGW (2010). Animal research: reporting in vivo experiments: the ARRIVE guidelines. Br J Pharmacol 160**:** 1577-1579.

Krall N, da Cruz FP, Boutureira O, & Bernardes GJ (2016). Site-selective protein-modification chemistry for basic biology and drug development. Nat Chem 8**:** 103-113.

Ladwig GP, Robson MC, Liu R, Kuhn MA, Muir DF, & Schultz GS (2002). Ratios of activated matrix metalloproteinase-9 to tissue inhibitor of matrix metalloproteinase-1 in wound fluids are inversely correlated with healing of pressure ulcers. Wound Repair Regen 10**:** 26-37.

Li X, Wang C, Xiao J, McKeehan WL, & Wang F (2016). Fibroblast growth factors, old kids on the new block. Semin Cell Dev Biol 53**:**155-167.

Maddaluno L, Urwyler C, & Werner S (2017). Fibroblast growth factors: key players in regeneration and tissue repair. Development 144**:**4047-4060.

McGrath JC, & Lilley E (2015). Implementing guidelines on reporting research using animals (ARRIVE etc.): new requirements for publication in BJP. Br J Pharmacol 172**:** 3189-3193.

Nguyen TH, Kim SH, Decker CG, Wong DY, Loo JA, & Maynard HD (2013). A heparin-mimicking polymer conjugate stabilizes basic fibroblast growth factor. Nat Chem 5**:** 221-227.

Olekson MA, Faulknor R, Bandekar A, Sempkowski M, Hsia HC, & Berthiaume F (2015). SDF-1 liposomes promote sustained cell proliferation in mouse diabetic wounds. Wound Repair Regen 23**:** 711-723.

Parnaud G, Tache S, Peiffer G, & Corpet DE (1999). Polyethylene-glycol suppresses colon cancer and causes dose-dependent regression of azoxymethane-induced aberrant crypt foci in rats. Cancer Res 59**:** 5143-5147.

Potente M, Gerhardt H, & Carmeliet P (2011). Basic and therapeutic aspects of angiogenesis. Cell 146**:** 873-887.

Rabuka D (2010). Chemoenzymatic methods for site-specific protein modification. Curr Opin Chem Biol 14**:** 790-796.

Rosen CB, & Francis MB (2017). Targeting the N terminus for site-selective protein modification. Nat Chem Biol 13**:** 697-705.

Sarabipour S, & Hristova K (2016). Mechanism of FGF receptor dimerization and activation. Nat Commun 7**:** 10262.

Schlessinger J, Plotnikov AN, Ibrahimi OA, Eliseenkova AV, Yeh BK, Yayon A*, et al.* (2000). Crystal structure of a ternary FGF-FGFR-heparin complex reveals a dual role for heparin in FGFR binding and dimerization. Mol Cell 6**:** 743-750.

Slack JM, Darlington BG, Heath JK, & Godsave SF (1987). Mesoderm induction in early Xenopus embryos by heparin-binding growth factors. Nature 326**:** 197-200.

Takahashi K, & Yamanaka S (2006). Induction of pluripotent stem cells from mouse embryonic and adult fibroblast cultures by defined factors. Cell 126**:** 663-676.

van Horssen R, Galjart N, Rens JA, Eggermont AM, & ten Hagen TL (2006). Differential effects of matrix and growth factors on endothelial and fibroblast motility: application of a modified cell migration assay. J Cell Biochem 99**:** 1536-1552.

Xu HL, Chen PP, Wang LF, Tong MQ, Ou ZH, Zhao YZ*, et al.* (2018). Skin-permeable liposome improved stability and permeability of bFGF against skin of mice with deep second degree scald to promote hair follicle neogenesis through inhibition of scar formation. Colloids Surf B Biointerfaces 172**:** 573-585.

Zhou J, Cai X, Huang X, Dai Y, Sun L, Zhang B*, et al.* (2017). A novel glucagon-like peptide-1/glucagon receptor dual agonist exhibits weight-lowering and diabetes-protective effects. Eur J Med Chem 138**:** 1158-1169.

Figure Legends

Figure 1

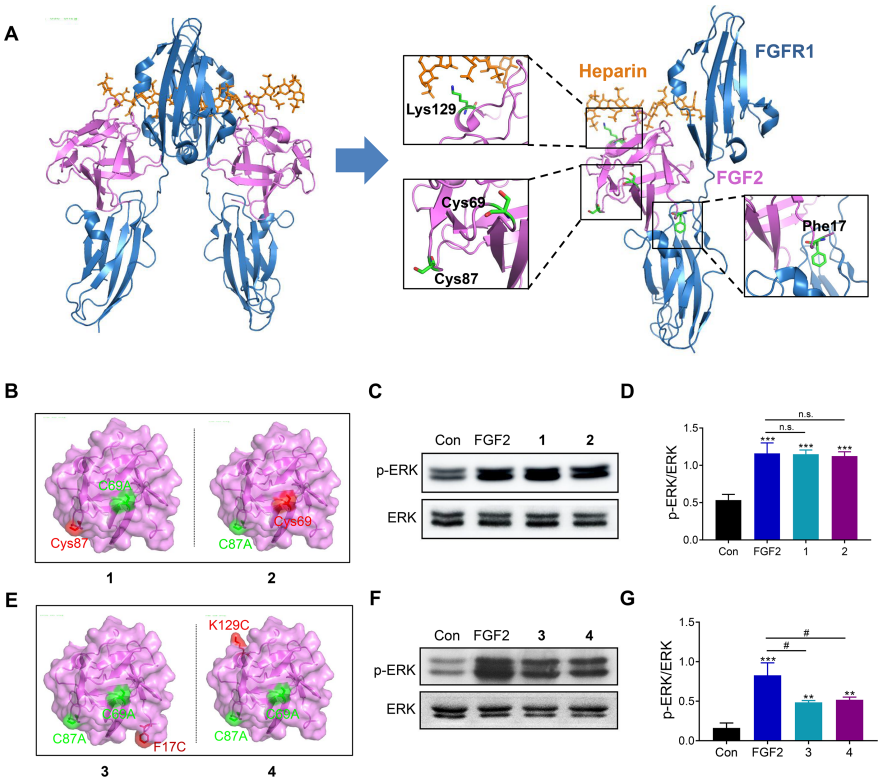

Figure 1. Design and activity analysis of native FGF2 and its variants. (**A**) Based on the crystal structure of FGF2 (PDB ID: 1FQ9), FGF2-FGFR1-heparin complex structure (left panel), close-up view of two surface-exposed residues, Lys129 and Phe17, near the heparin- and receptor-binding regions, respectively, and two surface-exposed cysteines (Cys69 and Cys87) on FGF2 (right panel). (**B**) Schematic representation of two FGF2 variants, including $FGF2^{C69A}$ (**1**) and $FGF2^{C87A}$(**2**). The residues labeled in green indicate mutation sites, and the residues marked in red are single conjugation sites for each FGF2 variant. (**C**) Immunoblotting analysis of p-ERK1/2 and ERK1/2 levels in cell lysates of HUVECs after treatment with compounds **1** , **2** (10 ng·mL^{-1}). ERK was used as a loading control (n = 3). (**E**) Schematic representation of another two synthetic FGF2 variants, including $FGF2^{C69A/C87A/F17C}$ (**3**) and $FGF2^{C69A/C87A/K129C}$ (**4**). (**F**) Immunoblotting analysis of p-ERK1/2 and ERK1/2 levels in cell lysates of HUVECs after treatment with compound **3** , **4** (10 ng·mL^{-1}) (n = 3). (**D, G**) Quantitative analysis of p-ERK1/2 in the indicated

groups. Data are displayed as means ± SEM. $^{**}P < 0.01$,$^{***}P < 0.001$ vs. control group;$^{\#}P < 0.05$ vs. FGF2 group; n.s., no significance.

Figure 2

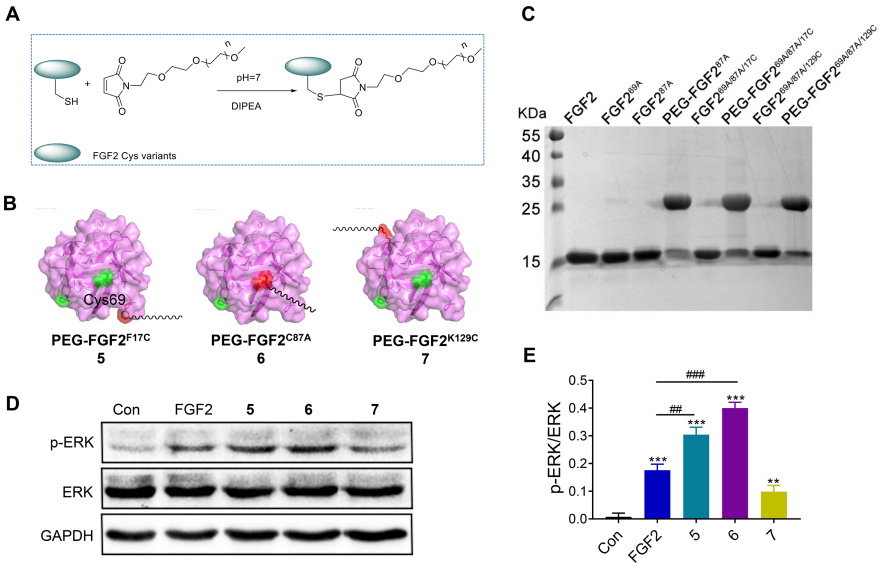

Figure 2. Preparation and activity analysis of PEGylated FGF2 conjugates. (**A**) Synthetic route of site-specific PEGylation using mPEG-Maleimide (mPEG-MAL, 5kDa). (**B**) Schematic representation of three FGF2 conjugates resulted from PEGylation, including PEG-FGF2^{F17C} (**5**), PEG-FGF2^{C87A} (**6**) and PEG-FGF2^{K129C} (**7**). (**C**) SDS-PAGE analysis of these PEG-FGF2 conjugates and native FGF2 under the optimal conditions. (**D**) Immunoblotting analysis of p-ERK1/2 and ERK1/2 levels in HUVECs after stimulation with PEG-FGF2 conjugates and FGF2 (10 ng·mL^{-1}). ERK and GAPDH were used as the loading controls (n = 3). (**E**) Quantitative analysis of p-ERK1/2 in the indicated groups. Data are displayed as means ± SEM.$^{**}P < 0.01$,$^{***}P < 0.001$ vs. control group;$^{\#}P < 0.05$,$^{\#\#}P < 0.01$ vs. FGF2 group.

Figure 3

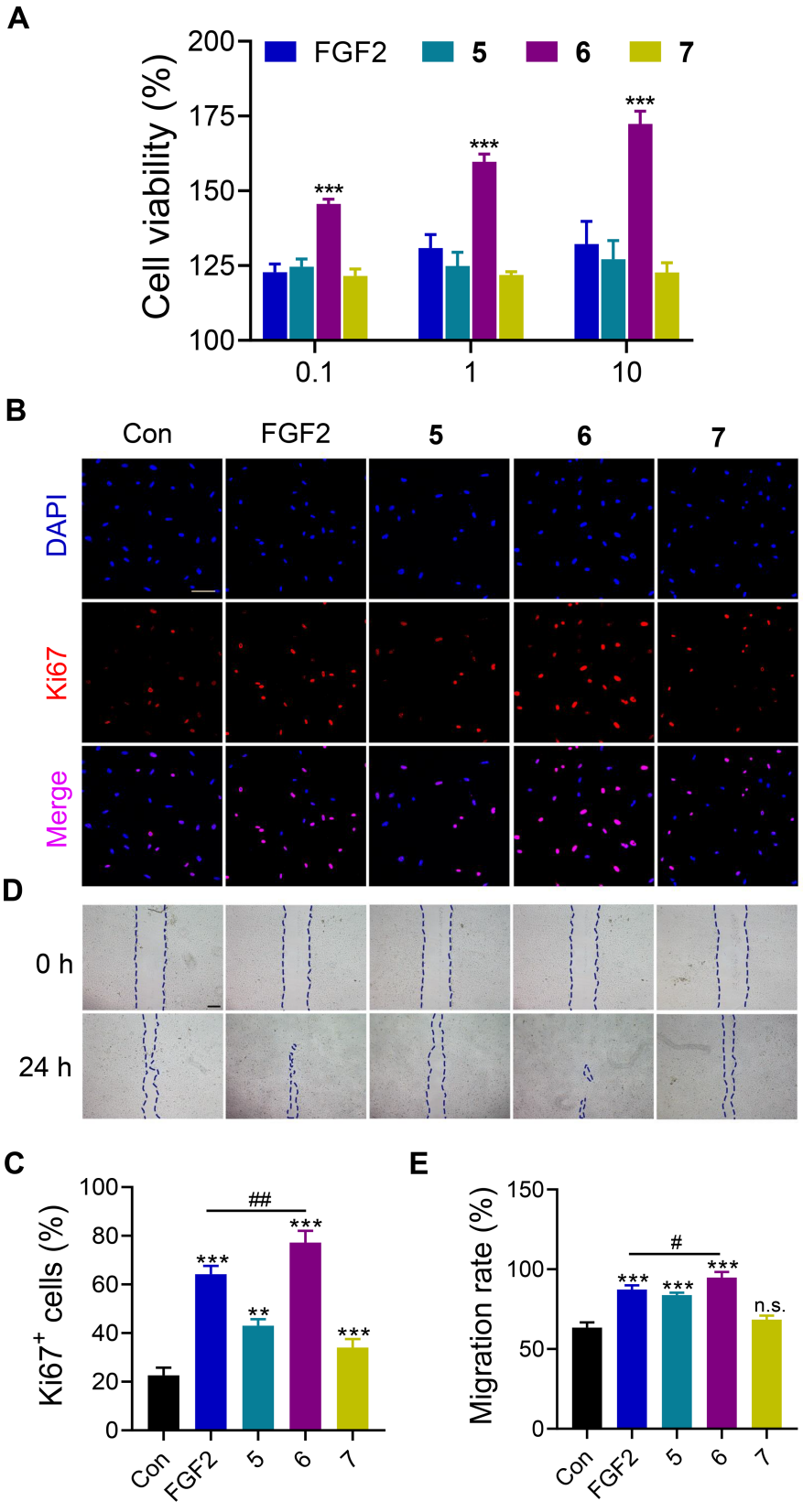

Figure 3. Effect of PEG-FGF2 conjugates on promoting proliferation and migration of HUVECs. (**A**) Percent cell viability of HUVECs after treatment with various concentrations of PEG-FGF2 conjugates, FGF2, and PBS (control), as determined by CCK-8 assay. (**B**) Representative images of immunofluorescence staining of Ki67 positive HUVECs (red). Nuclei were stained with DAPI (blue). Scale bar = 200 μm. (**C**) Quantitative analysis of Ki67-positive HUVECs (n = 5). $^{**}P < 0.01$,$^{***}P < 0.001$ vs. control group;$^{\#\#}P < 0.01$ vs. FGF2 group. (**D, E**) Scratch wound healing assay of HUVECs in the indicated groups for 24 h. The red dotted lines represent the wound boundary. Scale bar = 100 μm (n = 5). All data are displayed as means ± SEM.$^{***}P < 0.001$ vs. control group;$^{\#}P < 0.05$ vs. FGF2 group; n.s., no significance.

Figure 4

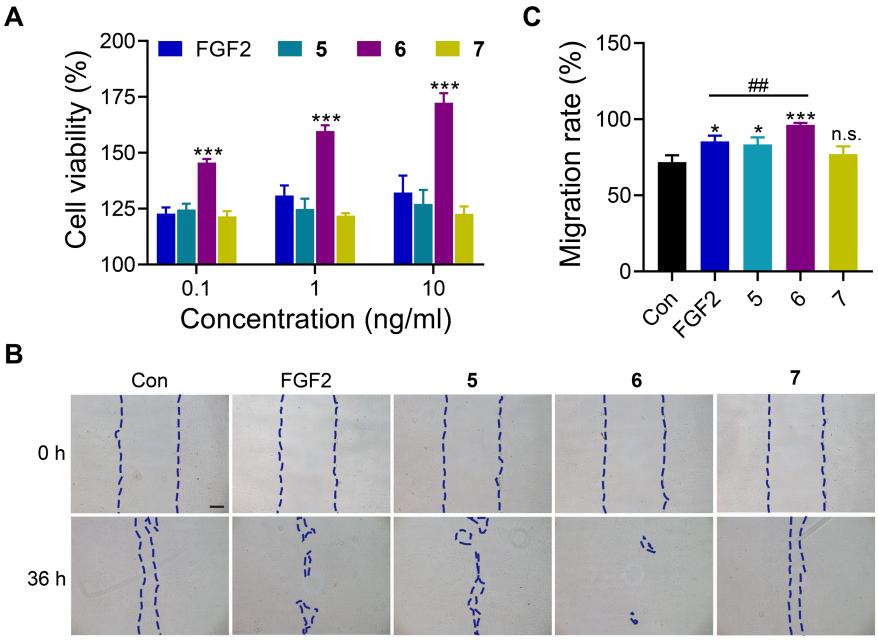

Figure 4. PEG-FGF2 conjugates promote the migration and proliferation of HDFs *in vitro*. (**A**) Cellular proliferation activity of PEG-FGF2 conjugates was determined by CCK-8 assay using HDF cells. $^{***}P < 0.001$ vs. control group. Scale bar = 200 μm. (**B, C**) Scratch wound healing assay of HDFs in the indicated groups for 36 h. The red dotted lines represent the wound boundary. Scale bar = 100 μm.$^{*}P < 0.05$,$^{***}P < 0.001$ vs. control group;$^{\#\#}P < 0.01$ vs. FGF2 group; n.s., no significance. All data are displayed as means ± SEM of 5 independent experiments.

Figure 5

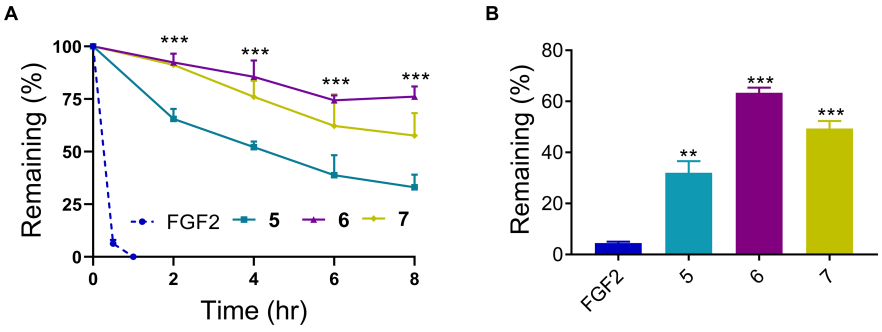

Figure 5. Stability of PEG-FGF2 conjugates in Rat plasma and wound fluid. (**A**) The remaining levels of FGF2 and PEG-FGF2 conjugates in rat plasma at indicated time points.$^{***}P < 0.001$ vs. FGF2 group. (**B**) The remaining levels of FGF2 and PEG-FGF2 conjugates determined by ELISA kit after incubation for 24 h with wound fluids.$^{**}P < 0.01$,$^{***}P < 0.001$ vs. control group. All data are displayed as means ± SEM of 3 independent experiments.

Figure 6

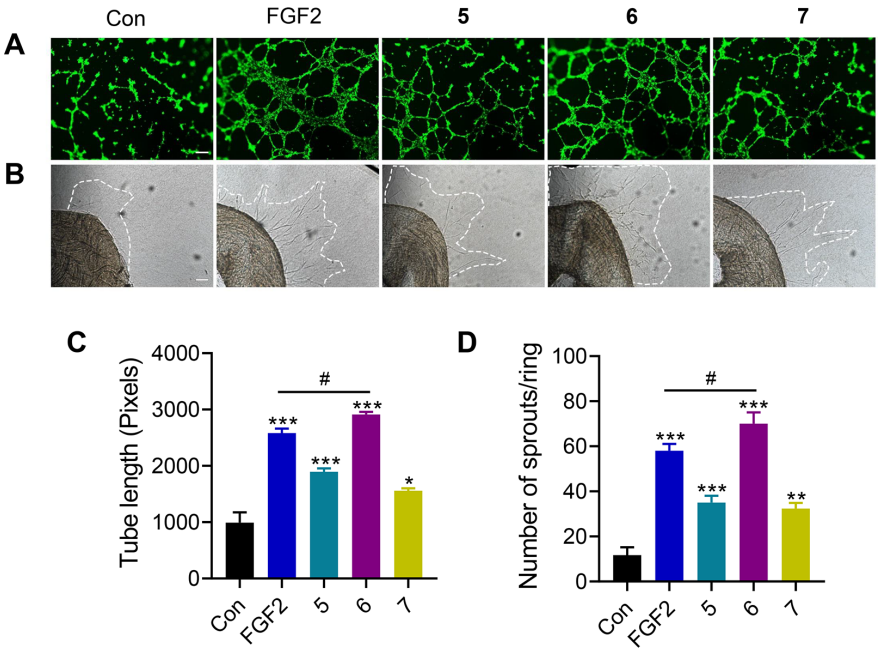

Figure 6. Effect of PEG-FGF2 conjugates to promote angiogenesis*in vitro* and *ex vivo*. (**A**) Capillary-like tube formation was assessed by Matrigel angiogenesis assay in HUVECs. Cells were cultured in HG (33 mM) in the presence of FGF2 or PEG-FGF2 conjugates (10 ng·mL^{-1}) for 72 h. (**B**) Representative images of aortic rings from C57BL/6 mice. Dotted lines indicate the visual field of sprouts. Quantitative analysis of tube length in (**C**) and the number of sprouts in (**D**). Scale bars = 300 μm. $^{*}P < 0.05$,$^{**}P < 0.01$,$^{***}P < 0.001$ vs. control group;$^{\#}P < 0.05$ vs. FGF2 group. All data are displayed as means ± SEM of 5 independent experiments.

Figure 7

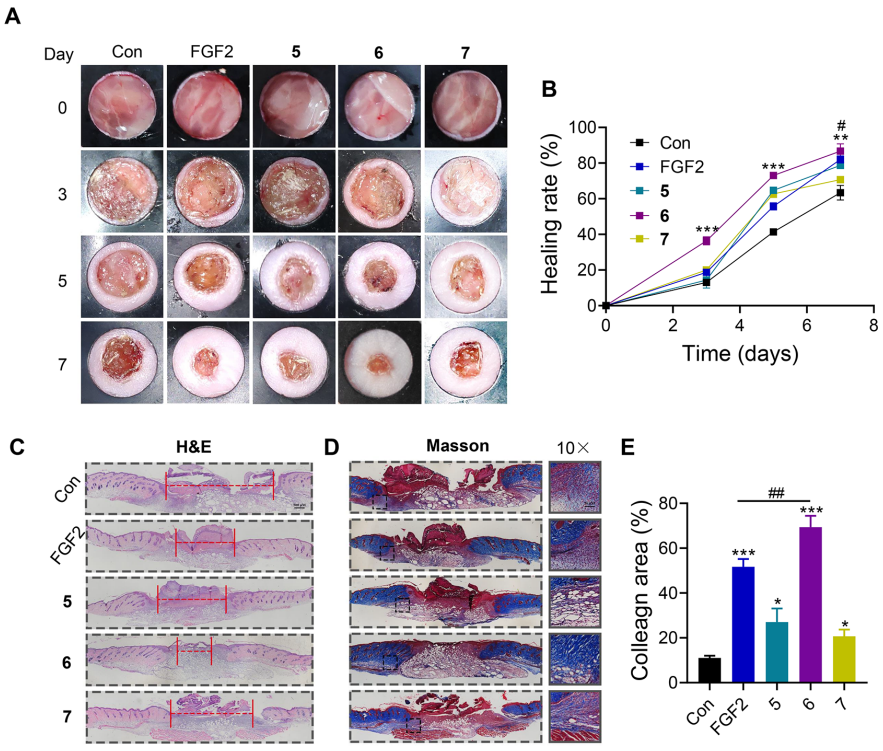

Figure 7. ***In vivo*** **assessment of PEG-FGF2 conjugates on skin wound healing.** (**A**) Representative images of wounds in mice after treatment with FGF2, compound **5** , **6** ,**7** and PBS at day 0, 3, 5 or 7 post-wounding. (**B**) The calculated wound closure rates in each group at the indicated time points. $^{**}P < 0.01$,$^{***}P < 0.001$ vs. control group;$^{\#}P < 0.05$ vs. FGF2 group. (**C**) H&E histology of representative wound sections at day 7 after surgery. The wound margin is indicated by red dashed line. Scale bar = 500 μm. Masson's trichrome staining of wound tissues in (**D**) and the percentage of relative collagen areas in (**E**). $^{*}P < 0.05$,$^{***}P < 0.001$ vs. control group;$^{\#\#}P < 0.01$ vs. FGF2 group. All values displayed are means ± SEM of 5 independent experiments.

Figure 8

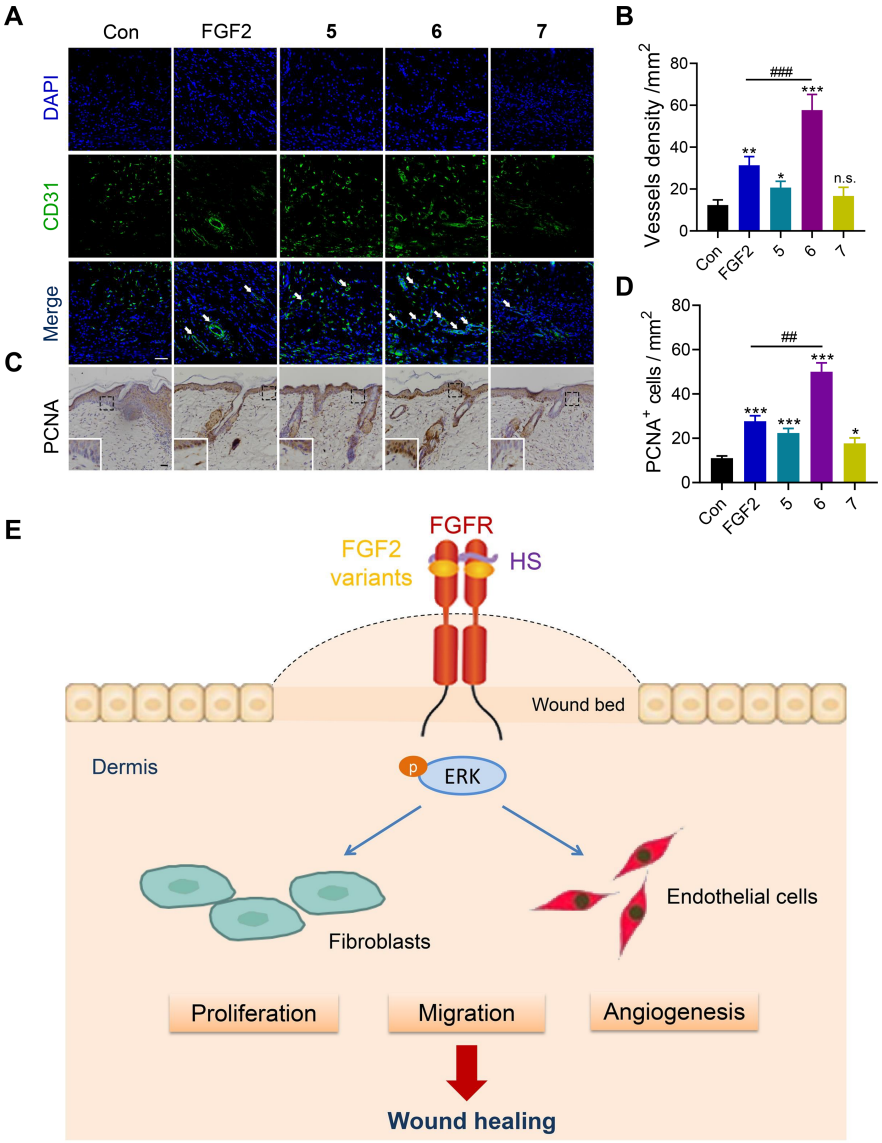

Figure 8. Promotion of angiogenesis and proliferation on wound skin tissues. (**A**) Representative immunofluorescence images of CD31 (green) and DAPI (blue) staining of wound skin tissues. White arrows indicate the newly formed blood vessels. Scale bars = 300 μm. (**B**) Quantitative analysis of the number of blood vessels per mm^2. (**C**) Immunohistochemistry (IHC) staining of PCNA positive cells in wound skin tissues. (**D**) The numbers of PCNA positive cells. $^{*}P < 0.05, ^{**}P < 0.01, ^{***}P < 0.001; ^{\#\#}P < 0.01, ^{\#\#\#}P < 0.001$ vs. FGF2 group; n.s., no significance. All values displayed are means ± SEM of 5 independent experiments. (**E**) Schematic illustration of the designed PEG-FGF2 conjugates that can promote cell proliferation, migration and angiogenesis via FGFR-ERK signing pathway in cutaneous wound.

Hosted file

`Supplemental table.docx` available at https://authorea.com/users/316793/articles/446935-structure-guided-pegylated-fibroblast-growth-factor-2-variants-accelerate-wound-healing-with-improved-stability